Materials Transactions, Vol. 43, No. 3 (2002) pp. 575 to 579

Relationship Between the Liquidus Surface and Structures of Zr–Cu–Al Bulk Amorphous Alloys

Yoshihiko Yokoyama[1], Hiroshi Inoue[1], Kenzo Fukaura[1] and Akihisa Inoue[2]

[1]*Faculty of Engineering, Himeji Institute of Technology, Shosha, Himeji 671-2201, Japan*
[2]*Institute for Materials Research, Tohoku University, Katahira, Aobaku, Sendai 980-8577, Japan*

By using a Al_2O_3 cell coated with Si_3N_4, the melting point (T_m) of the cast bulk amorphous samples were measured on DTA curves cooled from the molten state. Based on the T_m data, the partial liquidus surface of Zr–Cu–Al ternary alloys was determined. A ternary eutectic point is located around $Zr_{50}Cu_{40}Al_{10}$, and low melting temperatures of less than 1273 K were obtained in a wide compositional area of 40–70 at%Zr, 30–60 at% Cu and 0–10 at%Al. Bulk amorphous alloys in Zr–Cu–Al ternary system were produced by an arc-casting method and the highest tensile strength of 2000 MPa was observed in $Zr_{50}Cu_{40}Al_{10}$.

(Received November 14, 2001; Accepted January 28, 2002)

Keywords: *liquidus surface, isothermal section, zirconium-copper-aluminum alloy system, ternary eutectic point, bulk amorphous alloy, mechanical properties*

1. Introduction

The glass-forming ability of Zr-based bulk amorphous alloys can be evaluated by the wide temperature range of supercooled liquid region[1)] before crystallization because all bulk amorphous alloys have been obtained in the alloy composition in which the wide supercooled liquid region is observed. In the Zr–Cu–Al ternary alloy system, a $Zr_{65}Cu_{25}Al_{10}$ amorphous alloy[2)] has a rather large ΔT_x ($= T_x - T_g$) of about 80 K, and cylindrical bulk amorphous rods with a diameter of centimeter size have been produced.[3)] However, the large supercooled liquid region does not always mean high glass-forming ability. In the production of a bulk shape amorphous alloy, the glass-forming ability is also dominated by T_m/T_g.[4)] Consequently, the liquidus temperature is also an important parameter to dominate the forming-ability of bulk amorphous alloy.

On the other hand, the cast structure of bulk amorphous alloy is merely depend on the phase diagrams, because a high melting (eutectic) temperature brings about a thermal affect as exemplified structural relaxation embrittlement, and a steep slant liquidus surface region means the including a inclusion particles in the melt before casting. In order to produce a ductile perfect bulk amorphous alloy, the phase diagrams of the alloy should be examined. Based on the systematically investigation of amorphous alloys, it has been recognized that the multiplication[5)] of alloy components leads to a much wider supercooled liquid region which can be regarded as an increase of glass-forming ability in Zr–Cu–Ni–Al[6)] alloy system. However, the existence of micrometer sized crystalline inclusions often results in inferior mechanical properties or accidental fracture.[7)] The elimination of such crystalline inclusions may increase the ductility of bulk amorphous alloys. The formation of crystalline inclusion is thought to originate from impurities in molten alloy before casting. The data on liquidus surface and isothermal sections are important to obtain information on crystalline inclusions in the molten alloy before casting.

This paper intends to determine liquidus surface and isothermal section and to examine relation between liquidus surface and primary crystallized phases of Zr–Cu–Al bulk amorphous alloys. Furthermore, based on the liquidus surface and isothermal sections, Zr–Cu–Al bulk amorphous alloys were prepared by an arc-casting method and mechanical properties was examined.

2. Experimental Procedure

Ternary Zr–Cu–Al (Zr = 20–75 at%, Cu = 20–70 at% and Al = 10–40 at%) alloy ingots were prepared by arc melting pure Zr, Cu, Al, and Ni elements in an argon atmosphere. The alloy ingots were completely remelted, and cast into cylindrical rod samples with diameters of ϕ3 mm and ϕ10 mm, and a length of 70 mm by an arc-casting method.[8)] The cast structure was examined by scanning electron microscopy (SEM), and the compositions of several phases in the quenched samples were determined by an electron probe microanalyzer (EPMA). The melting temperatures of the samples were measured by differential thermal analysis (DTA) in an argon atmosphere. In the DTA measurement, Al_2O_3 cell was covered with Si_3N_4 ceramic to avoid the oxidization between the molten alloy and cell. The tensile testing was examined by an Instron tensile testing machine with wire resistance strain gage measurement apparatus at initial strain rate of $6.7 \times 10^{-3}\,s^{-1}$. The hardness was measured by micro Vickers testing machine with a 2.9 N for a loading time of 15 sec.

3. Results and Discussion

It is difficult to determine an equilibrium melting temperature in the Zr–Cu–Al alloys because of their large supercooling ability. In general, the melting temperature should be measured under a constant slow cooling rate from the melt. Since the melting temperature of the Zr-based alloys depend on cooling rate and alloy composition, the true melting temperature cannot be determined by this measurement method. Consequently, we tried to measure a melting temperature at a constant slow heating rate. The bulk amor-

phous or quenched crystalline samples were cast into cylindrical rods (ϕ3 mm × 50 mm) by the copper mold casting process. The cast sample was enveloped Zr-foil for degassing and then melted in a high-purity Ar atmosphere. The sample in the DTA measurement was covered with thin oxidized husk, which supports the molten alloy so as not to flow over on the cell. A homogeneously mixed alloy melt can be obtained at temperatures as low as possible. Figure 1 shows a DTA curve of the $Zr_{50}Cu_{40}Al_{10}$ bulk amorphous alloy measured at the heating and cooling rates of 0.67 and 1.6×10^{-2} K/s, respectively. In the heating DTA curve, the amorphous phase transforms to a crystalline one at the first exothermic peak, and the refuse temperature defined by the sharp bending point on the DTA curve is about 1198 K, and the further heating up to 1300 K is necessary to obtain a homogeneously mixed melt. On the other hand, in the cooling DTA curve, cooling rate is as low as 1.6×10^{-2} K/s to avoid supercooling in the Zr–Cu–Al alloys. The binary and ternary eutectic reactions are 1124 K and 1120 K, respectively, indicating that the $Zr_{50}Cu_{40}Al_{10}$ composition is close to the ternary eutectic point. Figure 2 shows the composition regions of intermetallic compounds in Zr–Cu–Al ternary system.[9] Binary Zr–Al compounds have an enormous solubility of Cu element, because of easy substitution of Cu for Al. These binary Zr–Al compounds have high melting temperatures. Consequently, the liquidus temperature increases drastically, when the composition approaches the formation regions of these Zr–Al(Cu) compounds. Figure 3 shows a partial liquidus surface of the Zr–Cu–Al alloys. The liquidus surface indicates an important feature of this alloy system. That is, one can see a wide compositional range of 40–70 at%Zr, 30–60 at%Cu and 0–10 at%Al, where the low melting temperatures are less than 1273 K. The ternary eutectic point appears to lie around $Zr_{50}Cu_{40}Al_{10}$ within the compositional region with low melting temperature. The exact composition of the ternary eutectic point was not determined because of much significant supercooling ability of this alloy. As shown in Fig. 2, the liquidus surface temperature increases drastically with increasing Al content from 10 to 15 at%.

Glass-forming ability has been evaluated by ΔT_x value, because large ΔT_x value implies high resistance against crystallization. Inoue *et al.* have proposed that bulk glass-forming ability is originated in the special alloys, which satisfy the following three factors; (1) multicomponent consisting of more than three elements, (2) significant atomic size mismatches above 12%, (3) negative mixing enthalpy between elements. Figure 4 shows compositional dependence of ΔT_x values in the Zr–Cu–Al alloys.[2] The $Zr_{65}Cu_{25}Al_{10}$ alloy with larger ΔT_x value is expected to have high glass-forming ability. In addition to the stability of supercooled liquid, a supercooling ability is another important factor. Large supercooling is usually seen at the composition near eutectic

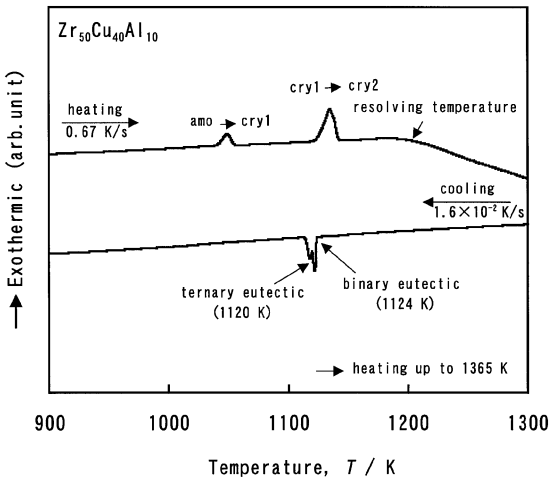

Fig. 1 DTA curves of the $Zr_{50}Cu_{40}Al_{10}$ bulk amorphous alloy measured at the heating and cooling rate of 0.67 and 2.8×10^{-4} K/s.

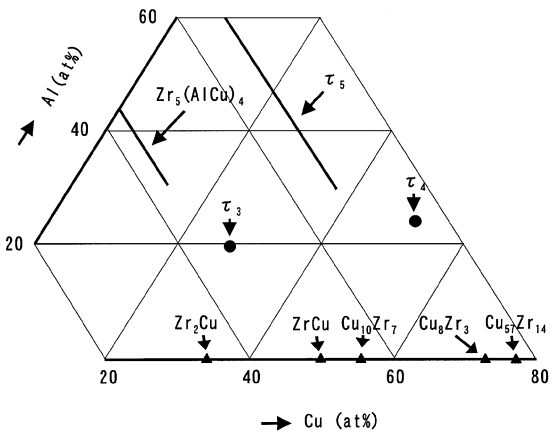

Fig. 2 Isothermal section at 1073 K for Zr–Cu–Al ternary alloys.[9]

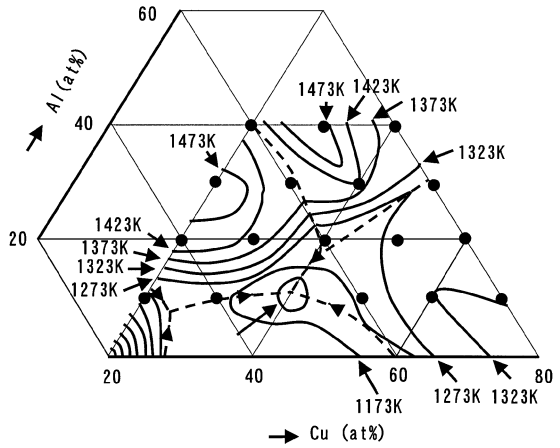

Fig. 3 Liquidus surface of Zr–Cu–Al ternary alloys.

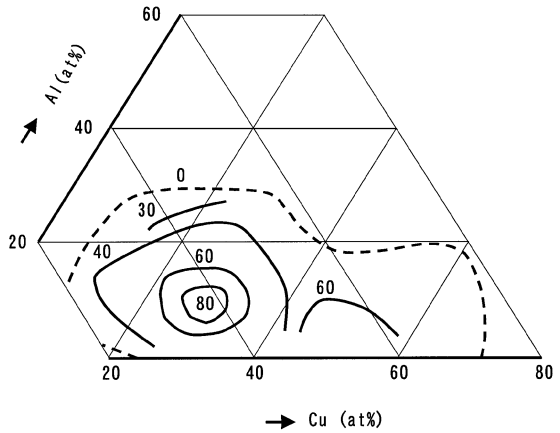

Fig. 4 Constitution dependence of supercooled liquid region (ΔT_x) of Zr–Cu–Al ternary amorphous alloys.[2]

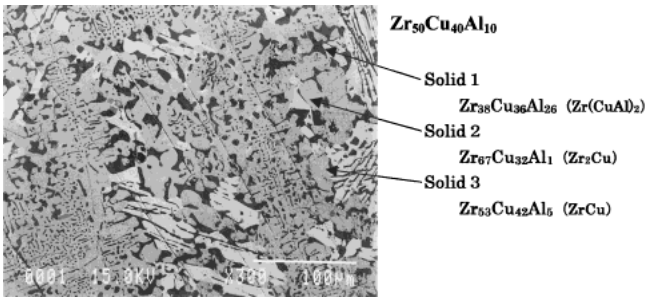

Fig. 5 SEM image of the slowly solidified $Zr_{50}Cu_{40}Al_{10}$ alloy.

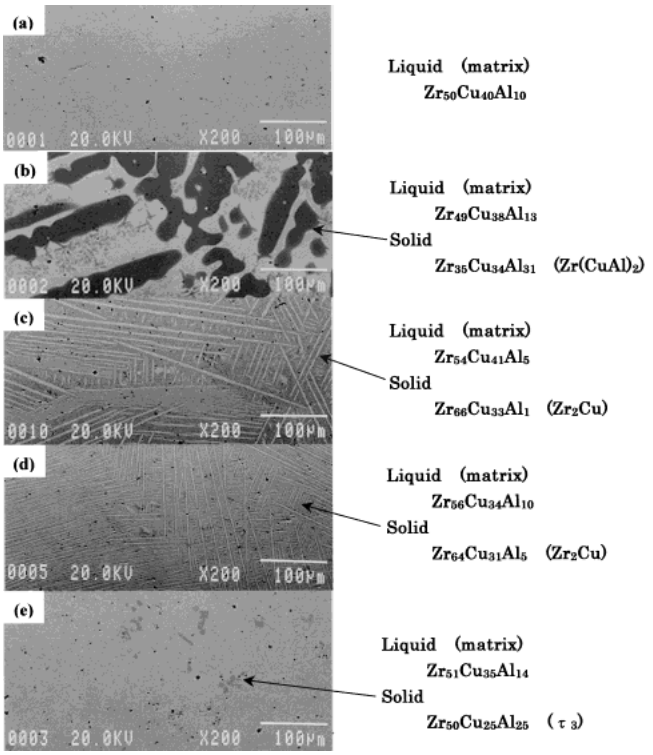

Fig. 6 SEM images of the water quenched samples after annealing at 1173 K and EPMA analyzed compositions of each phases.

point. Consequently, the liquidus surface is significant factor to produce a large sized bulk amorphous alloy without any crystalline inclusions. Figure 5 shows a SEM image of the slowly cooled $Zr_{50}Cu_{40}Al_{10}$ alloy. The SEM image consists of three different phases; 1) $Zr_{38}Cu_{36}Al_{26}$ ($Zr(CuAl)_2$, *black*), 2) $Zr_{67}Cu_{32}Al_1$ (Zr_2Cu, *white*) and 3) $Zr_{53}Cu_{42}Al_5$ (ZrCu, *gray*). Furthermore, the structure appears to have a complex lamellar mode of these three phases, indicating that this alloy is located near the ternary eutectic point.

In ordezr to control a molten alloy constitution, it is necessary to obtain the information on the relationship between liquid and solid phases, because the sort of primary crystalline phase depends on the compositional change. An optimum liquid composition, at which a liquid structure without crystalline particles is obtained even in a supercooling state, can be thought to exist in the Zr–Cu–Al system. In the Zr–Cu–Al bulk amorphous alloys, dendritic τ_3 crystalline inclusions act as an initiation of fracture. That is, the dendritic τ_3 crystalline inclusions bring about fatal embrittlement of the Zr-based bulk amorphous alloys. Consequently, clarifying the formation mechanism of τ_3 phase is an important work to

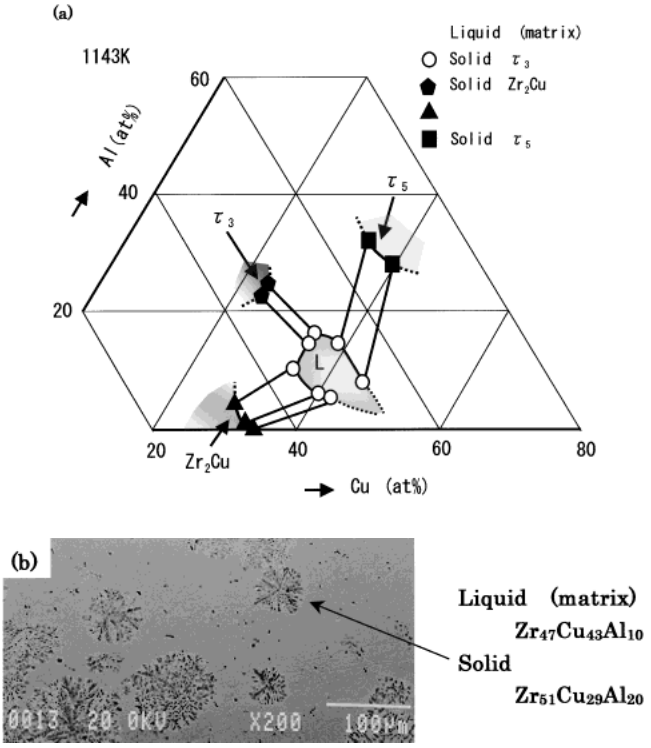

Fig. 7 Partial isothermal section at 1143 K for Zr–Cu–Al ternary alloys (a), and SEM image of the $Zr_{50}Cu_{40}Al_{10}$ water quenched sample from 1143 K containing a small amount of oxygen (b).

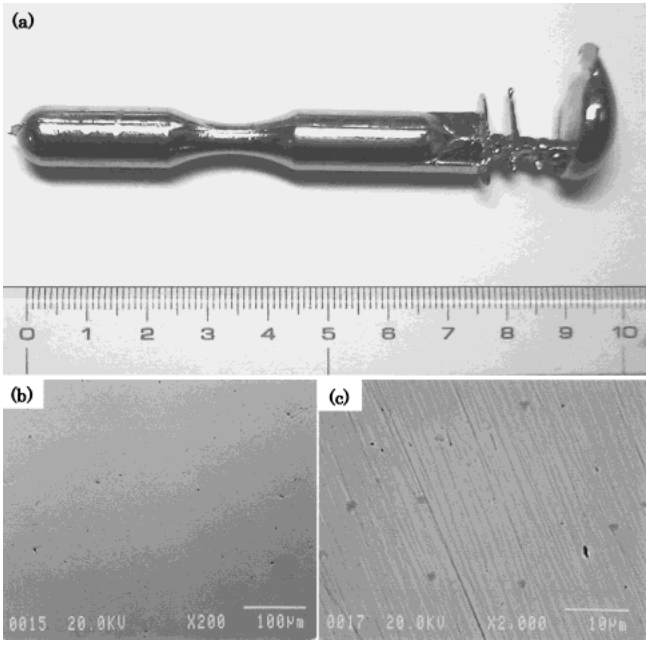

Fig. 8 The arc-casting $Zr_{50}Cu_{40}Al_{10}$ bulk amorphous alloy (a), and its SEM image with low magnification (b) and high magnification (c).

eliminate the inclusions in the molten Zr–Cu–Al alloy before casting. Figure 6 shows SEM images of some Zr–Cu–Al samples subjected water quenching after annealing at 1173 K together with the compositional analysis data on liquid (chilled fine structure or amorphous) and solid phases examined by EPMA. In Fig. 6 the analyzed compositions of the liquid and individual solid phases are also denoted at the right-hand. No second phase is observed in the $Zr_{50}Cu_{40}Al_{10}$ bulk amorphous

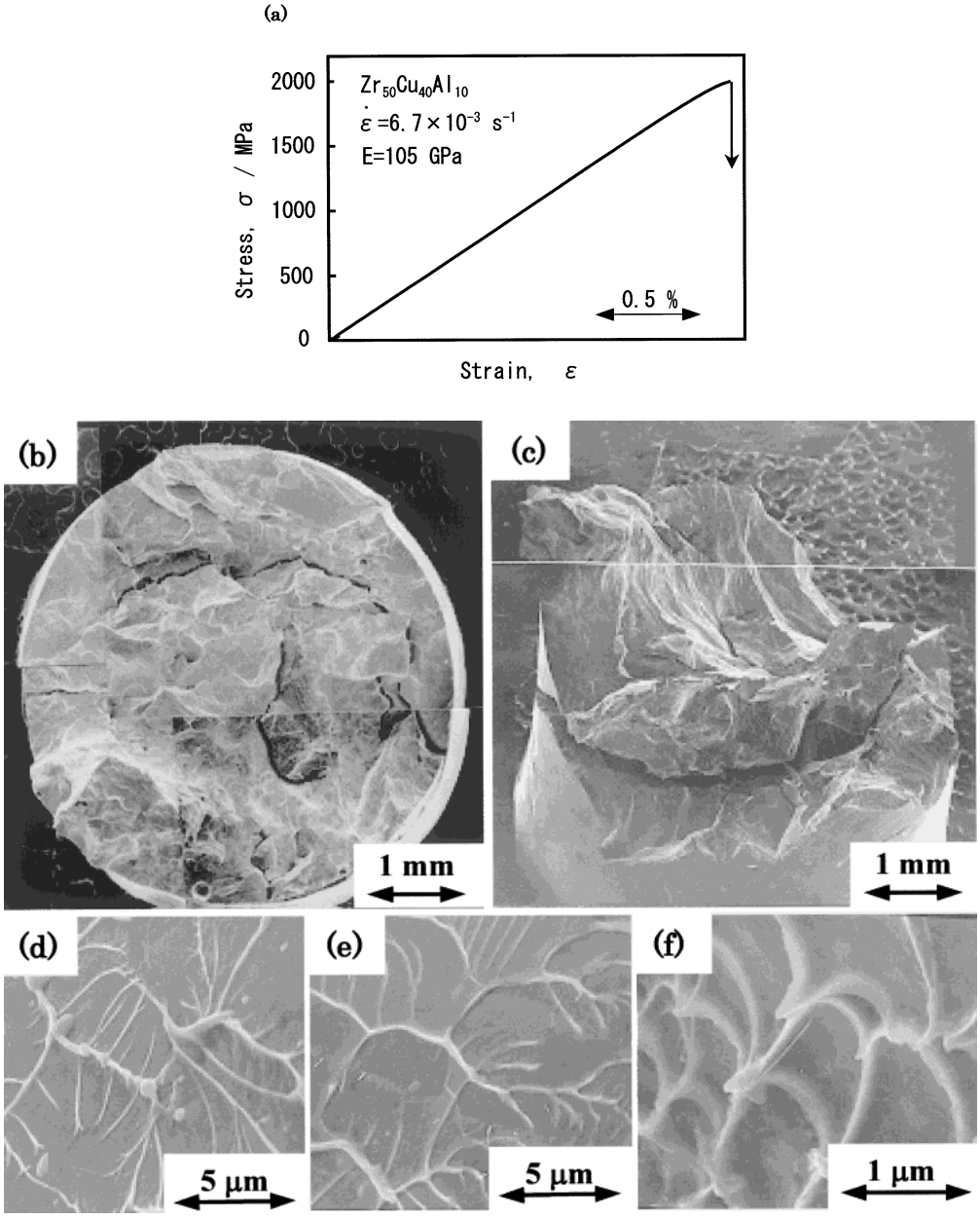

Fig. 9 Tensile stress-strain curve of the arc-casting $Zr_{50}Cu_{40}Al_{10}$ bulk amorphous alloy (a), and SEM images (b) to (f) of the tensile fractured surface.

sample as shown in Fig. 6(a). In Figs. 6(b), (c) and (d), one can see well grown primary crystals of $Zr(CuAl)_2$ and Zr_2Cu. The primary crystal particles were observed in the localized region, because the primary crystals crystallized inhomogeneously. However, the τ_3 primary crystallized particles were observed homogeneously in the sample as shown in Fig. 6(e). The τ_3 phase has a rectangular parallelepiped shape. These SEM images in Fig. 6 reveal that the high glass-forming ability may be obtained for the $Zr_{50}Cu_{40}Al_{10}$ alloy. The 1143 K isothermal section was constructed by writing the tie line relationship between the solid and liquid phases as shown in Fig. 6. Figure 7 shows a partial 1143 K isothermal section of Zr–Cu–Al ternary system. The liquid composition, which is in equilibrium with τ_3 phase, is located in the Al-enriched area. However, the shape of the τ_3 inclusions in the water-quenched sample is not dendrite but cubic as shown in Fig. 6(e). The dendritic τ_3 inclusions are observed in a slightly oxidized sample as shown in Fig. 7(b). Consequently, the dendritic growth of τ_3 inclusions seems to be caused by the oxygen, which was dissolved in the bulk amorphous alloys.

The $Zr_{50}Cu_{40}Al_{10}$ alloy had a superior glass-forming ability among the master alloys examined in the present work. The $Zr_{50}Cu_{40}Al_{10}$ master alloy ingot consists of an almost amorphous single phase, and a small part of crystallized area is seen in the bottom side. Therefore, we produced a $Zr_{50}Cu_{40}Al_{10}$ bulk amorphous sample by the arc-casting method. Figure 8(a) shows outer appearance of the arc-casting $Zr_{50}Cu_{40}Al_{10}$ bulk amorphous alloy. The arc-casting method is characterized by the mold shape with no restriction. As shown in Figs. 8(a), the dumbbell type tensile testing sample can be easily prepared by the arc-casting method. The structure of the cast sample is shown in Figs. 8(b) and (c). Figure 8(b) shows no crystalline inclusions, but in high-magnified range, some particle shaped crystalline inclusions

with diameters of 1 to 2 μm are seen as shown in Fig. 8(c). However the cast tensile sample exhibits high tensile strength up to 2000 MPa. The tensile strength is higher than the previous data in Zr–Al–TM (TM: Cu, Ni, Co) alloy systems[6,10] as about 300 MPa. Figure 9(a) shows tensile stress-strain curve of the cast sample at a strain rate of $6.7 \times 10^{-3}\,s^{-1}$. The Young's modulus of 105 GPa is slightly higher than that of ordinary Zr-based bulk amorphous alloys. In the tensile stress-strain curve, a small amount of plastic elongation is seen after yielding. The plastic deformation can be recognized from the fractured surface structure. The SEM images of the whole fractured surface are shown in Fig. 9 as front (b) and side (c) views. The fractured surface consists of many steep slipped planes and secondary fractured crevices. This fact implies that the many slip planes were suddenly enhanced at the same time and interrupted each other. The conflict operation among the slip bands brings about a slight plastic elongation before fracture. In general, the fractured surface of bulk amorphous alloys consists mainly of a single slipped plane along a maximum shear stress direction. The macroscopic fractured surface of the arc-casting sample is more complex. However, the microscopic fractured surface of the arc-casting sample is covered by well developed vein pattern as shown in Figs. 9(d), (e) and (f). The generation of appreciable plastic elongation of the arc-casting $Zr_{50}Cu_{40}Al_{10}$ bulk amorphous alloy is promising for improvements of ductility and fatigue strength of bulk amorphous alloys. The origin for the difference in the fractured surface between the arc-casting sample and ordinary bulk amorphous sample remains unclear in this work. The present data indicate that the bulk amorphous alloy with high strength can be prepared by the simple arc-casting method even in the principle Zr–Cu–Al ternary alloy system.

4. Summary

The liquidus surface and isothermal section in Zr–Cu–Al ternary system were examined and the data were used to determine the alloy composition. Oxide inclusions in the bulk amorphous alloy have great effect on the formation of dendritic crystalline inclusions, which act as an initiation of crack and fracture. The results obtained are summarized below.

(1) A ternary eutectic point is located around $Zr_{50}Cu_{40}Al_{10}$.

(2) The Zr–Cu–Al alloys in the wide compositional region of 40–70 at%Zr, 30–60 at%Cu and 0–10 at%Al have low melting temperatures of less than 1273 K.

(3) The arc-casting $Zr_{50}Cu_{40}Al_{10}$ bulk amorphous alloy exhibits good mechanical properties, *i.e.*, tensile strength of 2000 MPa, Young's modulus of 105 GPa and Vickers hardness of 580.

REFERENCES

1) A. Inoue, T. Zhang and T. Masumoto: Mater. Trans., JIM **32** (1991) 599–604.
2) A. Inoue, D. Kawase, A. P. Tsai, T. Zhang and T. Masumoto: Mater. Sci. Eng. **A178** (1994) 255–263.
3) A. Inoue, T. Zhang and T. Masumoto: Mater. Trans., JIM **39** (1998) 318–321.
4) A. Inoue: Mater. Trans., JIM **36** (1995) 866–875.
5) A. Inoue, T. Shibata and T. Zhang: Mater. Trans., JIM **36** (1995) 1420–1426.
6) A. Inoue, T. Zhang and T. Masumoto: Mater. Trans., JIM **36** (1995) 391–398.
7) A. Pecker and W. L. Johnson: Appl. Phys. Lett. **63** (1993) 2342–2344.
8) Y. Yokoyama, K. Fukaura, H. Sunada, K. Tkagi and K. Kikuchi: Materia Japan **3** (2000) 275–277.
9) V. Ya Markiv and V. V. Burnashova: Poroshk. Metall. **12** (1970) 53–58.
10) A. Inoue and T. Zhang: Mater. Trans., JIM **36** (1995) 1184–1187.